

# StrokeNet: An automated approach for segmentation and rupture risk prediction of intracranial aneurysm



Muhammad Irfan <sup>a</sup>, Khalid Mahmood Malik <sup>a,\*</sup>, Jamil Ahmad <sup>b</sup>, Ghaus Malik <sup>c</sup>

<sup>a</sup> SMILES LAB, Department of Computer Science and Engineering, Oakland University, Rochester, MI, 48309, USA

<sup>b</sup> Department of Computer Vision, Mohamed Bin Zayed University of Artificial Intelligence (MBZUAI), Abu Dhabi, United Arab Emirates

<sup>c</sup> Executive Vice-Chair at Department of Neurosurgery, Henry Ford Health System, Detroit, MI, USA

## ARTICLE INFO

## ABSTRACT

### Keywords:

Computer-aided diagnosis  
Medical image analysis  
Features fusion intracranial  
Aneurysm rupture  
Prediction segmentation  
Subarachnoid Hemorrhage (SAH)

Intracranial Aneurysms (IA) present a complex challenge for neurosurgeons as the risks associated with surgical intervention, such as Subarachnoid Hemorrhage (SAH) mortality and morbidity, may outweigh the benefits of aneurysmal occlusion in some cases. Hence, there is a critical need for developing techniques that assist physicians in assessing the risk of aneurysm rupture to determine which aneurysms require treatment. However, a reliable IA rupture risk prediction technique is currently unavailable. To address this issue, this study proposes a novel approach for aneurysm segmentation and multidisciplinary rupture prediction using 2D Digital Subtraction Angiography (DSA) images. The proposed method involves training a fully connected convolutional neural network (CNN) to segment aneurysm regions in DSA images, followed by extracting and fusing different features using a multidisciplinary approach, including deep features, geometrical features, Fourier descriptor, and shear pressure on the aneurysm wall. The proposed method also adopts a fast correlation-based filter approach to drop highly correlated features from the set of fused features. Finally, the selected fused features are passed through a Decision Tree classifier to predict the rupture severity of the associated aneurysm into four classes: Mild, Moderate, Severe, and Critical. The proposed method is evaluated on a newly developed DSA image dataset and on public datasets to assess its generalizability. The system's performance is also evaluated on DSA images annotated by expert neurosurgeons for the rupture risk assessment of the segmented aneurysm. The proposed system outperforms existing state-of-the-art segmentation methods, achieving an 85 % accuracy against annotated DSA images for the risk assessment of aneurysmal rupture.

## 1. Introduction

Intracranial or cerebral aneurysms refer to localized deformities of the arterial walls in the brain. These aneurysms can develop at various locations in the Circle of Willis, and are classified based on their size, shape, and phenotype (Ivantsits et al., 2022). As noninvasive brain imaging becomes increasingly accessible, the early detection rate of unruptured intracranial aneurysms (UIA) has witnessed significant growth, with further increase anticipated. Although most UIAs do not rupture, the consequences of rupture are severe, resulting in high mortality and morbidity. In the USA, an UIA ruptures every 18 min on average, leading to 30,000 annual cases of subarachnoid hemorrhage (SAH) with a 40 % fatality rate (BAF Statistics, 2023). Survivors of a SAH often experience permanent neurological disabilities, affecting approximately 66 % of cases (Ajiboye et al., 2015; Brinjikji et al., 2016). While

the majority of UIAs remain stable and do not rupture, the ramifications of a rupture can result in a life-threatening condition (An et al., 2022).

Neurosurgeons face a complex decision-making process when determining the management approach for asymptomatic unruptured intracranial aneurysms (UIAs) for following reasons. While clinical guidelines typically prioritize treatment for UIAs larger than 7 mm in size, it is noteworthy that small aneurysms (< 5 mm) account for 41 % of cases involving subarachnoid hemorrhage (SAH), whereas a considerable number of larger aneurysms do not undergo rupture. Surgical treatments can eliminate the risk of SAH but carry significant risks and potential complications. The decision to pursue early treatment must consider the risk of side effects versus the risk of SAH if the UIA is left untreated. Therefore, optimal patient care involves treating only those aneurysms that are likely to rupture. Currently, the prevailing approach for predicting brain aneurysm rupture involves manual assessment

\* Corresponding author.

E-mail address: [mahmood@oakland.edu](mailto:mahmood@oakland.edu) (K.M. Malik).

relying on the expertise of a neurosurgeon and limited utilization of PHASES and UIATS scores. But independent evaluation of these scores has proven to be poor predictors of rupture (Feghali et al., 2021; Malik et al., 2023). Unfortunately, a reliable method for assessing IA rupture risk has not yet been developed. Hence, developing a reliable IA rupture risk prediction technique is essential to assist clinicians in making informed decisions about the management of patients with intracranial aneurysms.

Over the last few years, a number of challenges have been organized to address the detection and analysis of aneurysm rupture. Notably, the ASME 2013 Challenge (Steinman et al., 2013) and subsequent CFD-based rupture risk estimation challenges (Janiga et al., 2015) have been held. However, limited confidence in the clinical community regarding the accuracy of CFD methods (Rahmany and Khilifa, 2014) prompted the recent ADAM challenge at MICCAI 2021, which focused exclusively on detection and segmentation using deep learning techniques (Timmins et al., 2021). Despite the fact that clinically available data is predominantly 2D, the AI research community has mostly pursued intracranial aneurysm detection using 3D image analysis. As such, 2D image-based rupture prediction using deep learning methods remains an underexplored research domain.

While 2D Magnetic Resonance Angiography (MRA), Computed Tomographic Angiography (CTA), and Digital Subtraction Angiography (DSA) are the primary diagnostic

methods for aneurysm, DSA is considered to be the gold standard. Differentiating aneurysms from loops of blood vessels in DSA is very challenging, as shown in Fig. 1.

Although hemodynamics and CFD community has performed some preliminary work, no thorough automated image analysis work has been performed to predict and investigate aneurysm rupture risk using 2D-DSA image modality. Hemodynamics proves that geometry of aneurysm's feeding artery has shown significant role in pathophysiology and aneurysmal rupture. For instance, Zhou et al. (2017) studied the impact of shear stress for aneurysm rupture analysis and considers it as a predominant factor for rupture. Similarly, Cebral et al. (2011) studied flow patterns in the aneurysm and associated arteries in smaller impingement zones. Further, in CFD literature, the shape of the aneurysm is studied as well where some geometrical features show a strong correlation to aneurysm rupture analysis. A study reported by Kleinloog et al. (2018) pointed out 144 risk factors including size ratio, neck diameter, dome direction, and large volume-to-ostium ratio that could have potential use in clinical practice. Due to limitations such as the need to simplify aneurysm geometry, reliance on assumptions for computational feasibility, and the disregard for Fluid-Structure Interaction, using CFD alone for aneurysm rupture prediction is not sufficient. Consequently, it is essential to explore alternative techniques in order to enhance the accuracy and reliability of rupture prediction. Recently, deep learning methods have been used for aneurysm detection and segmentation (Dai et al., 2020). However, to date, no study exists that uses interdisciplinary features (i.e. Deep features, geometrical features, shape features, and blood flow patterns) extracted from 2D images to perform aneurysmal rupture analysis.

This paper utilizes 2D image analysis instead of 3D rotational DSA imaging due to its wider availability and lower cost. In comparison, 3D

rotational DSA imaging requires longer exposure to radiation, which may lead to complications for patients. While 2D DSA imaging is typically sufficient for routine diagnostic purposes, 3D rotational DSA imaging is reserved for cases where a detailed 3D visualization of the aneurysm is needed, such as in preoperative planning for endovascular treatment. Thus, the objective of this paper is to address the current gaps in predicting aneurysm rupture through the utilization of 2D-DSA. This paper aims to make the following contributions:

- Prior deep learning methods applied to medical imaging only focus on aneurysm detection and segmentation without rupture risk prediction. This paper proposes a framework for aneurysm detection, segmentation as well as rupture prediction using 2D DSA images.
- A novel customized end-to-end convolutional neural network (CNN) network is proposed which extracts effective features with fewer parameters to efficiently segment aneurysms and ignore vascular loops.
- To predict the risk of aneurysm rupture, our proposed framework integrates a variety of features extracted through Inception V3, geometrical features, Fourier descriptors, and blood flow patterns in the relevant arteries. To identify the most influential features, we employ the fast correlation-based filter (FCBF) approach and select an optimal subset. Finally, we utilize a Decision Tree classifier to categorize aneurysm criticality based on the identified features.

The rest of the paper is organized as follows: Section 2 summarizes the current literature on aneurysm segmentation and rupture prediction. Technical details for aneurysm segmentation and rupture prediction are described in Section 3. Section 4 evaluates the proposed method using a newly developed, DSA-based dataset. A discussion on the results is presented in Section 5, and Section 6 concludes the paper with future directions.

## 2. Related work

In the literature, there has been a significant emphasis on recent research efforts pertaining to cerebral aneurysm detection, segmentation, and prediction. However, the analysis of rupture risk in aneurysms has received comparatively less attention. Hence, this section reviews the related work on aneurysm segmentation and briefly discusses the notable works in the area of aneurysm risk prediction.

### 2.1. Aneurysm Segmentation

Segmentation of aneurysms from the parental vessel is essential for quantitative analysis and rupture prediction. Prior methods of aneurysm segmentation were based on vessel segmentation. The study by Wilson and Noble (1997), focuses on a statistical model optimized with an expectation-maximization algorithm for vessel segmentation. Further, Bogunović et al. (2011) utilizes geodesic active regions to improve execution time and is robust to changes in size ratios of the image modalities and image spatial resolution. Similarly, Nikravanshalmani et al. (2013) uses a multistage approach for saccular aneurysm segmentation. First, they use a CTA image to segment vessels using a region growing approach. Next, a seed point for the aneurysm is used to separate the affected vessel from the parental artery. Dakua et al. (2018) presents a two-step procedure using a stochastic resonance-based methodology in the discrete Hartley transform domain to improve the visual information in the CTA image. A multi-scale principal component analysis (PCA) is utilized to estimate the phase map, which is combined with a level set map to segment an aneurysm. Chen et al. (2020b) and Stember et al. (2019) utilize a U-Net model to segment vessel dilation. In comparison to the standard U-Net model, Zhang and Chen (2019), Dai et al. (2020), and Zeng et al., and Chen et al. (2020a) propose the DDNet, RCNN, and a 2.5D model, respectively, with improved detection rate. Patel et al. (2020) illustrate a slight improvement in the performance of the U-Net

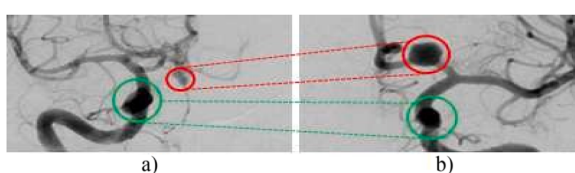


**Fig. 1.** Vascular loops and aneurysm in DSA images where the green color shows benign vascular loops, and the red color indicates an aneurysm. Note the similarities between the two-colored regions, which makes differentiation difficult for the untrained eye.

model over DeepMedic for aneurysm segmentation. HeadXNet, a novel approach for aneurysm segmentation is proposed by Park et al. (2019) which uses an encoder-decoder method and shows improved performance in aneurysm segmentation. Chen et al. (2020b) uses an “Active Contour” strategy for the segmentation of aneurysms located in a high contrast area. The method is based on “Eula Elastica” model, which fine-tunes the segmentation boundaries of the aneurysm. Rahmany and Khlifa (2014) study fuzzy approaches for intracranial aneurysm segmentation.

In recent years, there has been a growing interest in using different neural network models for diagnosing brain related diseases Rusak et al., 2022; Gan et al., 2021). Specifically, Convolutional Neural Networks (CNNs) have been explored for detecting aneurysms in 3D angiograms (Jerman et al., 2017). For example, Nakao et al. (2018) employed a CNN to extract deep features and identify the inside and outside voxels of an aneurysm. Zeng et al. (2019) used a sequence of 3D rotational angiogram (3D-RA) images and applied a spatial information fusion method, rather than a 3D-CNN, for segmenting intracranial aneurysms. Similarly, Sichtermann et al. (2019) and Shi et al. (2020) studied the same problem for MRA and CTA images, respectively. To overcome the limitation of insufficient data for intracranial aneurysm detection and segmentation, Yang et al. (2020) introduced an open-access 3D- intracranial dataset for training neural networks. However, all these methods focus solely.

on aneurysm detection or segmentation using 3D-MRA or CTA images. Furthermore, simulation tools are used to reconstruct a 3D model of the aneurysm to study wall deformation.

## 2.2. Aneurysm rupture prediction

In recent years, there has been a growing interest in the prediction of aneurysm rupture, as it can aid in the selection of patients who require treatment and can also help in the development of preventative strategies. One of the major challenges in the prediction of aneurysm rupture is the complex interplay between morphological and hemodynamic factors. Some studies have demonstrated the association between morphological and hemodynamic factors and the development and rupture of intracranial aneurysms. For instance, Tang et al. (2022) found that irregular shape, larger size, and lower flow stability were significantly associated with an increased risk of aneurysm rupture. Several studies have attempted to predict the risk of aneurysm rupture using these factors, including machine learning techniques (Walther et al., 2022; Stumpo et al., 2022). These studies have yielded encouraging outcomes, showcasing reasonable predictive accuracy on CTA modality.

Malik et al. (2018) proposed a morphological-based method for assessing the future rupture risk of aneurysms in DSA images. Zhai et al. (2018) utilized virtual reality and an Oculus Rift to reconstruct and analyze aneurysm growth in a 3D environment for real-time interactive environments and training purposes. Their method involved using Haar wavelet transformation and a threshold-based approach to segment an aneurysm in a DICOM image. Jerman et al. (2019) proposed an automated cutting plane method using Hough- and multi-hypothesis detection to determine the center of an aneurysm, measure its size, aspect ratio, dome height, and non-sphericity index. An et al. (2022) recently conducted a study on conventional features to predict aneurysm rupture risk, achieving an average of 0.78 F-2 score. However, this study utilized 3D-MRA images where an aneurysm’s regions were manually extracted to predict the rupture chances. All of these techniques extract features from the reconstructed 3D model of an aneurysm’s region. Furthermore, these methods do not take into account the geometrical aspect of an aneurysm, which is critical in aneurysm rupture analysis.

## 3. Proposed StrokeNet framework

As illustrated in Fig. 2, the proposed framework is divided into three modules: 1) Aneurysm Segmentation Network, 2).

Aneurysm Feature Extraction, and 3) Feature Selection for Rupture Prediction using Correlation-based Filters. Further, Section 3.1 discusses the network architecture used for segmentation, Section 3.2 describes the geometrical features, deep features, blood flow patterns, and Fourier descriptors and their significance in aneurysm rupture criticality. Section 3.3 presents the feature selection mechanism to eliminate highly correlated features and select independent features for SAH prediction.

### 3.1. Aneurysm Segmentation network

There exist several approaches for segmentation task in medical imaging (Minaee et al., 2021). Hence, taking those networks as a baseline, we proposed a customized network, as shown in step 1 of Fig. 2. In some medical images, especially in the case of aneurysms, the shapes of regions of interest are highly irregular and deteriorate overall model performance. Further, in DSA images, aneurysms and loops are difficult to differentiate due to the injected dye during DSA procedure, making the aneurysm look like loops as shown in Fig. 1. The misleading nature of loops in DSA images poses a significant challenge for segmentation networks, such as Long et al. (2014) in effectively identifying the region of interest, particularly in cases of aneurysms. Moreover, the imbalance

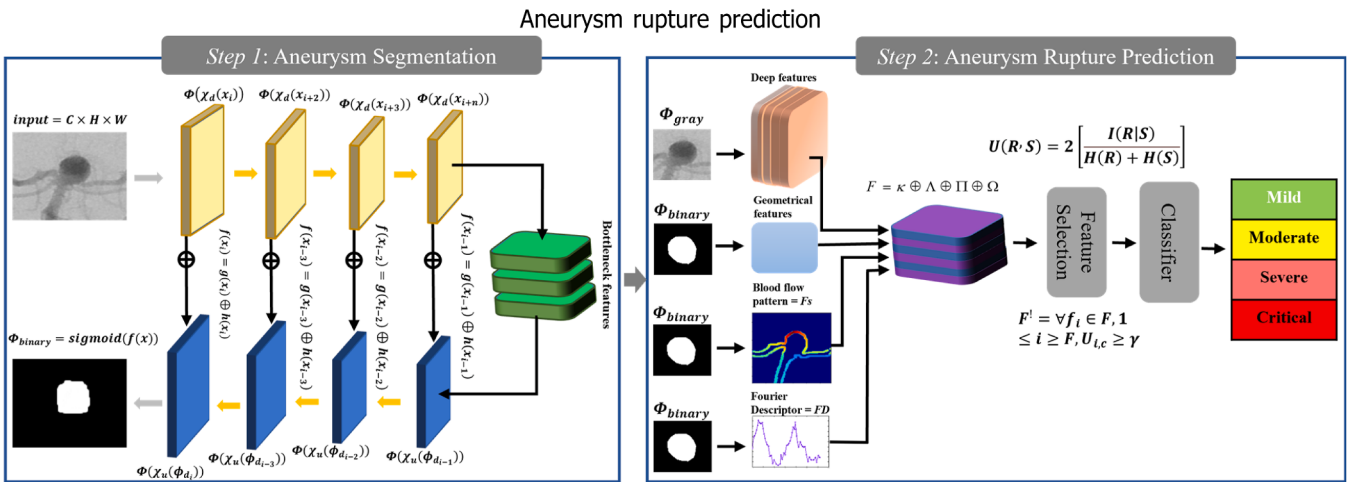


**Fig. 2.** Pictorial representation of the proposed framework for aneurysm segmentation and rupture prediction. Step 1 involves processing the input DSA image through the proposed end-to-end CNN to generate a segmented aneurysm. In Step 2, the deep features, geometrical features, Fourier descriptor, and blood flow patterns are extracted and fused together, denoted by  $F$ . Then, we eliminate highly correlated features using the fast correlation-based filter and form an independent feature set  $F'$ , which is then passed to the classifier to categorize the given aneurysm into four classes.

in the dataset due to the more frequent appearance of loops in images compared to aneurysms results in overfitting when using generic models. As a result, there is a rise in erroneous identification of loops as aneurysms, and the segmentation of the small aneurysm areas in the image is still challenging. Therefore, to address these issues, we proposed a customized end-to-end network that can effectively segment aneurysms while minimizing false detection of loops.

Let suppose, for a given input image  $x$  with  $C \times H \times W$  where  $C$ ,  $H$ , and  $W$  represent number of channels, height, and width, respectively. A convolution set of filter with  $\omega$  weights, we compute convolution of the first layer as:

$$\chi_{ab}^l = \sum_{a=0}^{m-1} \sum_{b=0}^{n-1} \omega_{ab} \Phi_{(i+a)(j+b)}^{l-1} \quad (1)$$

After each convolution, we take a region in each computed feature map and output a single value that is maximum in the respective region. If  $M \times N$  is the input feature map, then applying max pooling of  $k \times k$ , the output features map will be  $\frac{M}{k} \times \frac{N}{k}$ . Next, after each convolution, we apply the non-linearity as:

$$\Phi(x) = \varphi(\chi_{ij}) \quad (2)$$

Our model is based on encoder and decoder approach; hence, overall process of the model can be described as:

$$\begin{aligned} \phi_d &= \Phi(\chi_d^{(x)}) \\ \phi_u &= \Phi(\chi_u)(\phi_d) \end{aligned} \quad (3)$$

where  $\chi_u$  and  $\chi_d$  is the encoder and decoder to encode and decode feature maps, respectively. At the encoder side, the input is down sampled while increasing the channels maps with  $k$ -fold as:

$$\begin{aligned} g(x) &= \chi_u^l(x) \in R^{(C \times k)(H \times k)(W \times k)} \\ h(x) &= \chi_d^l(x) \in R^{\frac{C}{k} \times \frac{H}{k} \times \frac{W}{k}} \end{aligned} \quad (4)$$

where  $g(x)$  and  $h(x)$  represent the encoder and decoder. Further, we used features concatenation between the  $g(x)$  and  $h(x)$  as:

$$f(x_i) = g(x_i) \oplus h(x_i) \quad (5)$$

where  $f(x_i)$  represents the corresponding concatenated features map. In last,  $f(x)$  is passed from the sigmoid function to generate the predicted output mask as:

$$\phi_{binary} = sigmoid(f(x)) \quad (6)$$

where  $\phi_{binary}$  represents the binary mask of the segmented aneurysm. Further, details about number of features maps at encoder and decoder is given in the following subsections.

### 3.1.1. Encoding path

The proposed network architecture for aneurysm segmentation consists of encoding layers that include four steps. Each step involves two convolutional  $3 \times 3$  filters followed by  $3 \times 3$  max pooling and ReLU activation functions. The number of feature maps in successive layers grows two-fold, enabling the extraction of increasingly semantic features. To account for the relatively simpler overall structure of DSA images, where color and complex geometry are absent, the first layer extracts 16 feature maps. Subsequent layers have a reduced number of feature maps to avoid model overfitting. At the bottleneck, we reduced the number of features to 512 and maintained spatial dimensions at  $8 \times 8$  to enable the network to effectively encode pixel information related to the region of interest (aneurysms). This encoding process results in a segmented region that is highly accurate in terms of its shape.

### 3.1.2. Decoding path

The decoding step involves an up-sampling of  $2 \times 2$  convolutions, followed by ReLU activation and concatenation with the corresponding feature maps from the encoding path. The original image size is maintained during up-sampling to preserve features. In the final layer, a convolution of  $1 \times 1$  is applied to a 16-

component feature vector. Since we are dealing with binary data (aneurysm vs background), we found it more appropriate to use binary cross-entropy (BCE) as the loss function to measure the error and update the gradients using backpropagation. An ablation study evaluating the impact of various loss functions is presented in Section IV-B.

### 3.1.3. Blood flow pattern

Literature from CFDs suggest that hemodynamics especially blood flow is pivotal in aneurysm's tendency to rupture in specific areas of the arteries (Qiu et al., 2022). Consequently, blood flow in those arteries is considered to be a primary concern for most of the SAH risk estimation. In this study, we model the boundary of the aneurysm and the host artery as 2D finite elements. Further, each boundary pixel is considered as the finite element that gets affected by the incoming bloodstream through the aneurysm opening, incident at an angle. The response of each pixel to the incoming bloodstream (modelled as flowing in a straight line) is accumulated. To simulate the blood flow and estimate its effects on individual elements, we consider the blood flow to be Newtonian and define aneurysm opening between  $(x_1, y_1)$ , and  $(x_2, y_2)$  as shown in Fig. 3-(b). The slope  $m_o$  and angle  $\theta_o$  of the aneurysm opening is given by (7) whereas the blood flow slope  $m_b$  and angle  $\theta_b$  are computed as (8):

$$\begin{aligned} m_o &= \frac{y_2 - y_1}{x_2 - x_1} \\ \theta_o &= \tan^{-1}(m_o) \end{aligned} \quad (7)$$

$$\begin{aligned} m_b &= \frac{t_2 - t_1}{s_2 - s_1} \\ \theta_b &= \tan^{-1}(m_b) \end{aligned} \quad (8)$$

To find the impact of blood flow on the wall of aneurysm, the distance  $d_{ij}$  from the opening of the aneurysm to each element (boundary pixel) is computed and the impact score  $\sigma_{ij}$  for all aneurysm boundary pixels as:

$$\begin{aligned} d_{ij} &= \sum_i \sum_j \sqrt{(c_x - p_i)^2 (c_y - p_j)^2} \\ \sigma_{ij} &= \sum_i \sum_j \frac{K}{C + ((\theta_b - \theta_o))} \times d_{ij} \end{aligned} \quad (9)$$

where  $\sigma_{ij}$  represent the impact score at an element located at  $(i, j)$  on the aneurysm wall,  $(c_x, c_y)$  is an element on the aneurysm opening,  $(p_i, p_j)$  is the location of aneurysm boundary pixels, and  $K$  is a normalization constant. We consider that blood flow stress  $\sigma_{ij}$  is maximum on the region of aneurysm that forms a complete angle to the blood flow and  $\sigma_{ij}$  is minimum on aneurysm region when there is a reflex angle to the blood flow as shown in the Fig. 3.

In addition to blood flow pattern, we also extract shape-based features of the aneurysm in frequency domain using Fourier descriptors. Firstly, the boundary of the aneurysm is modeled as a centroid distance function (CDF), where the distance of each element is computed from the centroid of the aneurysm. A centroid distance histogram is computed where the bins represent angles, and the values correspond to distance of the element from the centroid.

$$CDF_0 = \sqrt{(x(n) - gx)^2 + (y(n) - gy)^2} \quad (10)$$

To make the  $CDF_0$  invariant to scale and orientation, we compute its

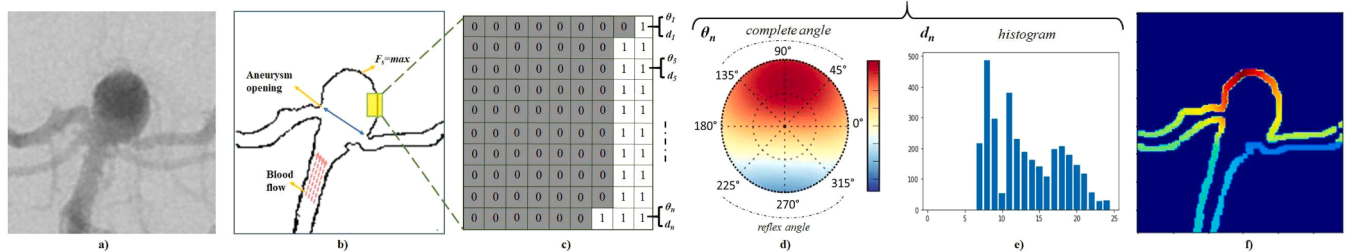


**Fig. 3.** Stress  $F_S$  of the blood flow on the wall of aneurysm where a) shows the input DSA image, b) shows the segmented region of aneurysm, c) shows the inverted image and the angle  $\theta_n$  and distance  $d_n$  of the aneurysm boundary, d) shows the heat map of the  $\theta_n$ , e) shows the histogram of distance  $d_n$ , and f) shows the final stress  $F_S$  on the wall of aneurysm.

Fourier transform and normalize the frequencies by the DC component of the spectrum. For a given image, (supposing that it's normalized to  $N$ ), the Fourier descriptor is given by:

$$v_n = \frac{1}{N} \sum_{i=1}^N CDF_{\theta_i} e^{-j\frac{2\pi i}{n}}, n = 1, 2, \dots, N-1 \quad (11)$$

where  $v_n$ ,  $n = 1, 2, \dots, N-1$  is the coefficient and is usually called Fourier descriptor (FD) of the aneurysm shape obtained after normalization using the DC component  $v_0$ . For easy understanding, in this study, the FD of the aneurysm shape is denoted by  $\Omega$ .

### 3.1.4. Geometrical features

Geometrical features have been studied in medical image analysis for a wide range of challenging medical imaging classification problems. In addition, there has been increasing interest in developing methods to predict the risk of rupture in patients with aneurysms. Recent clinical studies have shown that certain geometric features, such as aneurysm size, shape, and aspect ratio, can be used to predict the risk of rupture. For example, larger aneurysms and those with irregular shapes and high aspect ratios are more likely to rupture. In addition, the location of the aneurysm within the arterial tree can also influence the risk of rupture. Alongside, geometrical features and morphological analysis have also been studied for brain tumor (Zafar et al., 2019; Sharif et al., 2020) and lung nodules classification (Ye et al., 2009). It is evident that shape, size, and location of the aneurysm are crucial in their risk categorization. Hence, in our study, we investigated a new set of geometrical features for aneurysm shape analysis and studied their correlation with the criticality and rupture risk of an aneurysm. Keeping in view the geometry of a wide variety of aneurysms, in this study, we used seven geometrical shapes features including convex area (capturing shape irregularity), perimeter (aneurysm size), compactness, eccentricity, size ratio, neck diameter and aspect ratio (elongation).

### 3.1.5. Deep features

Recent studies have utilized CNN-based feature extraction techniques to analyze 3D-MRA and CTA images for various medical image domains. Wang et al. (2019) propose a deep learning method to classify lung nodules from CT images using transfer learning with the Inception V3 neural network architecture. In addition, Spanhol et al. (2016) use deep features for tumor classification in breast cancer histopathological images. Further, Meng et al. (2020) propose a deep learning method for segmenting cerebrovascular structures from DSA images using a multi-scale dense convolutional neural network (MSCNN). A similar study is also conducted by Labhane et al., (2020) that uses Inception V3 features to improve the performance of the model for detecting pediatric pneumonia. These studies showcase the potential of deep learning approaches in medical image analysis. In the proposed pipeline,

we used a set of deep features for aneurysm risk analysis. Our cross-fold validation showed that among three sets of models; VGG, ResNet, and Inception V3, the best performance was achieved on Inception V3 as the model can extract features at various scales and resolutions. Hence,

to supplement the geometrical features, the proposed algorithm uses the morphological features in conjunction with features extracted via Inception-v3 (Xia et al., 2017).

Overall, if a vector of deep features is represented by  $\kappa$ , normalized geometrical features by  $\Lambda$ , blood flow patterns by  $\Pi$ , and Fourier descriptor by  $\Omega$ , then set of fused features denoted by  $F$  is given by:

$$F = \kappa \parallel \Lambda \parallel \Pi \parallel \Omega \quad (12)$$

### 3.2. Features selection using correlation based filter

The previous section describes four very distinct feature classes: deep, geometrical, Fourier descriptor and blood flow patterns in order to find SAH criticality. Alone, neither of these features is sufficient as there is a high correlation of features between the given four classes. Our main goal is to drop highly correlated features among the classes and select distinct features that could help to predict aneurysmal criticality. Hence, in this section, we evaluate the goodness of various features and select specific features for aneurysm classification. In the case of an aneurysm rupture, a feature is considered good if it is highly relevant to a given class and is not redundant in any other class. In other words, if we take the correlation of two features as a good measure, the above suggestion will become that a selected feature is good only if it is highly correlated to the given class and less correlated to any other class.

For a linear correlation between a pair of variables ( $R, S$ ), the correlation  $c$  is given by:

$$c = \frac{\sum_i (r_i - \bar{r}_i)(s_i - \bar{s}_i)}{\sqrt{\sum_i (r_i - \bar{r}_i)^2} \sqrt{\sum_i (s_i - \bar{s}_i)^2}} \quad (13)$$

where  $r_i$  and  $s_i$  is the mean of  $R$ , and  $S$ , respectively, and  $c$  ranges between  $-1$  and  $1$ .  $R$  and  $S$  are totally independent, if  $c$  is zero otherwise  $R$  and  $S$  are completely depended. However, linear correlation between a pair of ( $R, S$ ) is not always safe, especially in real world values. In addition, linear correlation always require numerical values. To overcome these issues, for our set of features, we choose an entropy-based approach which is based on uncertainty of a random variables. Hence, entropy of  $R$  can be defined as:

$$H(R) = - \sum_i P(r_i) \log_2(P(r_i)) \quad (14)$$

and entropy of  $R$  over another variable  $S$  is given by:

$$H(R|S) = - \sum_i P(r_i) \sum_i P(r_i|s_i) \log_2(P(r_i|s_i)) \quad (15)$$

where  $P(r_i)$  is the prior probabilities of  $R$  and  $P(r_i|s_i)$  shows probabilities of  $R$  given  $S$ . The measure by which the entropy of  $R$  decreases gives auxiliary information about  $R$  given  $S$  called information gain (Quinlan, 2014), which is formulated as:

$$I(R|S) = H(R) - H(R|S) \quad (16)$$

According to (16), a given feature  $S$  is more correlated to  $R$  than  $Q$ , only if  $I(R|S) > I(Q|S)$  which is called symmetrical information gain. Hence, for our set of features, we select symmetrical uncertainty (Yu and Liu, 2003) as:

$$U(R, S) = 2 \left[ \frac{I(R|S)}{H(R) + H(S)} \right] \quad (17)$$

Eq. (17) normalizes the values between [0,1] where 1 predicts given feature  $R_i$  is the knowledge that completely predicts the class  $S_i$  and 0 if  $R_i$  is completely independent of given  $S_i$ .

Further, for a given data  $D$ , that contains a set of features.

$f = f_1, f_n$  for total classes  $C = C_1, C_n$ . Let  $\gamma$  be the good threshold that measures the correlation between  $f_i$  and given class  $C$ . Then a set of independent features  $F$  is given by  $\gamma$  such that  $\forall f_i \in F, 1 \leq i \leq n, U_{i,C} \geq \gamma$ . Hence, for a given feature  $F$ , if there exists feature  $f_j$  to a feature  $f_i$ , we consider it as the redundant feature and use  $F'$  to denote a set of redundant features and ignored it during the classification phase.

#### 4. Experimental evaluation

This section provides a detailed evaluation of the proposed work. First, the implementation details and datasets used for evaluation are discussed. Next, experiments are performed to evaluate the effectiveness of the proposed segmentation and rupture prediction techniques. To perform a comparative analysis of the proposed system with other state-of-the-art methods, a set of different metrics, including accuracy (ACC), precision ( $p$ ), recall ( $R$ ), and  $F$ -1 score are used. In addition to these metrics, we also use segmentation specific metrics, including mean intersection over union (mean IoU), pixel accuracy, and dice similarity coefficient (DSC) to compare the obtained results with other existing segmentation models. The experimental section is further divided into six subsections as follows: 4.1) Experimental Setup, 4.2) Hyperparameter setup, 4.3) Proposed Method Evaluation on 2D-DSA Images, 4.4) Comparison with Existing Segmentation Models, 4.5) Evaluation of Publicly Available Datasets, 4.6) Evaluation of blood flow patterns 4.7) Performance evaluation of FCBF with other features selection methods 4.8) Evaluation of various views/slices of aneurysm and 4.9) Analysis of various features set for aneurysm rupture classification.

##### 4.1. Experimental setup

The proposed system is implemented in Python 3.5 within a separate Anaconda environment. We utilized TensorFlow, Keras, and scikit-learn for model architecture specification training, and evaluation. Pre-processing was performed using OpenCV version 3.4.2.17 compiled with other necessary binaries. To visualize results and feature maps, we used the Python packages Matplotlib, scikit-image, and NumPy. All training and testing were conducted on Nvidia Tesla 4-GPUs with 16 GB ( $16 \times 4$ ) memory using CUDA version 10.0.1 and CuDNN version 7.6.

For training and evaluation, we collected a new dataset containing 408 DSA images spanning cases from 1997 to 2021 from the Henry Ford Health System following Institutional.

Review Board (IRB No. 11254) approval. The dataset was annotated by two board-certified neurosurgeons with extensive experience in the diagnosis and treatment of cerebral aneurysms. The annotations were done using a custom software tool that allowed for precise labeling of aneurysm regions and segmentation of the blood vessels. The tool also allowed for the labeling of different classes of aneurysms based on their size, shape, and location. The distribution of patients based on aneurysm location is illustrated in Table 2. The dataset includes 39 non-aneurysmal images and 369 unruptured aneurysmal images for aneurysm segmentation. In total, we used 408 images for the segmentation task, with 267 for training and 141 (including 39 non-aneurysmal images) for evaluation. We include non-aneurysm from the patients who had undergone cerebral angiography and selected those patients whose

radiologist review report confirm the absence of pathology. Moreover, based on the jpeg image of resolution  $1024 \times 1024$ , the average size of each risk class is illustrated in Table 1 where the size is measured on the assumption that ratio corresponds to aneurysm diameter in pixels. Additional details are provided in Table 1.

##### 4.2. Hyperparameter setup

One of the primary challenges of our study is to identify aneurysm-specific features using a CNN architecture. To achieve this, we conducted experiments using different formulations to train the proposed architecture and obtain various feature maps. These feature maps were then evaluated for their ability to distinguish between loops and aneurysms using a set of test images. The results of our experiments, including the details of the feature maps obtained via different formulations, are presented in Table 2.

Our proposed model architecture remained consistent across all experiments, with only the size of the feature maps, convolution kernels, and loss function changing. We observed,

that the use of mean squared error (MSE) as a loss function in Formulation 1 resulted in the worst performance, as shown in Fig. 4. Additionally, increasing the number of features at the bottom of the network led to overfitting, causing a reduction in overall accuracy and the detection of aneurysms as loops, as shown in Fig. 5.

Furthermore, we evaluated the performance of our proposed architecture in terms of increasing and decreasing the convolution layers inside the network, and monitored the mean IoU and DSC scores, as shown in Fig. 6. Based on our findings, we reduced the feature maps on both the encoding and decoding sides to 512, changed the strides, and added dropout. The best performance was obtained via our proposed.

architecture, which utilized binary cross entropy as a loss function and reduced strides to zero while implementing dropout of 0.1. Reducing the strides to zero allowed for more information to flow into the subsequent layers, resulting in less pixel information loss and superior performance.

##### 4.3. Evaluating the efficacy of proposed method on 2D-DSA

In this section, we assessed the efficacy of the proposed method using various image resolutions and augmentation techniques. Table 3 illustrates the IoU, pixel accuracy, and DSC scores for different sets of image resolutions. Additionally, Table 4 presents the  $P$ ,  $R$ ,  $F$ -score, and ACC scores for different experimental setups. For the first set of experiments, the best performance was achieved using an image resolution of  $256 \times 256$ , with accuracy and  $F$ -score of 80.97 % and 72.56 %, respectively. For the second set of experiments, we augmented the images using cropping, vertical and horizontal flipping, rotation, and translation. We generated 500 images, increased the batch size to 16, and repeated the experiments using the same configuration. In the second set, the best performance was obtained at a resolution of  $256 \times 256$

**Table 1**

Total number of patients and distribution of images per class.

Segmentation			
No. Patients	Training images	Testing images	Total images
186	267	141	408
Aneurysm criticality assessment			
Patient Type	Training images	Testing images	Total images
Mild	38	12	50
Moderate	56	18	74
Severe	78	22	100
Critical	56	17	73
Aneurysm size			
Mild	38	12	512-1792
Moderate	56	18	1793-2304
Severe	78	22	2304-3072
Critical	56	17	3072-above

**Table 2**

Distribution of aneurysm based on location.

Associated Artery	Patients
Anterior communicating artery	106
Basilar	47
Internal carotid artery	95
Middle cerebral artery	67
Posterior cerebral artery	21
Posterior communicating artery	20
Posterior inferior cerebellar artery	12
Superacclinoïd	32
Superior cerebellar artery	05

with scores of 0.81, 94.54 %, and 0.77 for average mean IoU, pixel accuracy, and DSC, respectively. Subsequently, we conducted the third and fourth sets of experiments by increasing the number of training images to 750 and 900 and the batch sizes to 24 and 32, respectively. However, we observed a gradual decrease in performance as the number of augmented images increased. One possible reason for the drop in accuracy could be the memorization of the data by the model due to the increased number of augmented images. The model may memorize the entire dataset instead of identifying patterns in the data, leading to good performance on the training data but poor performance on the validation set.

#### 4.4. Comparison with existing segmentation models

In recent years, Vision-based Transformers (ViT) have emerged as an

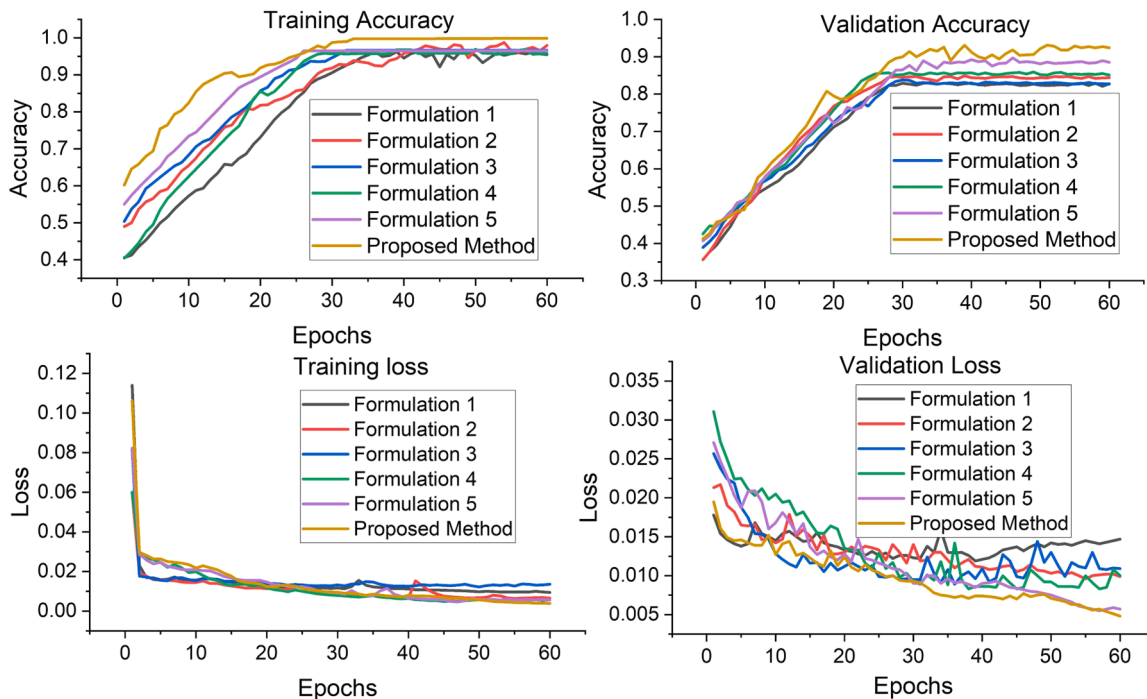


**Fig. 4.** Training and validation performance of the proposed segmentation network over different formulations.

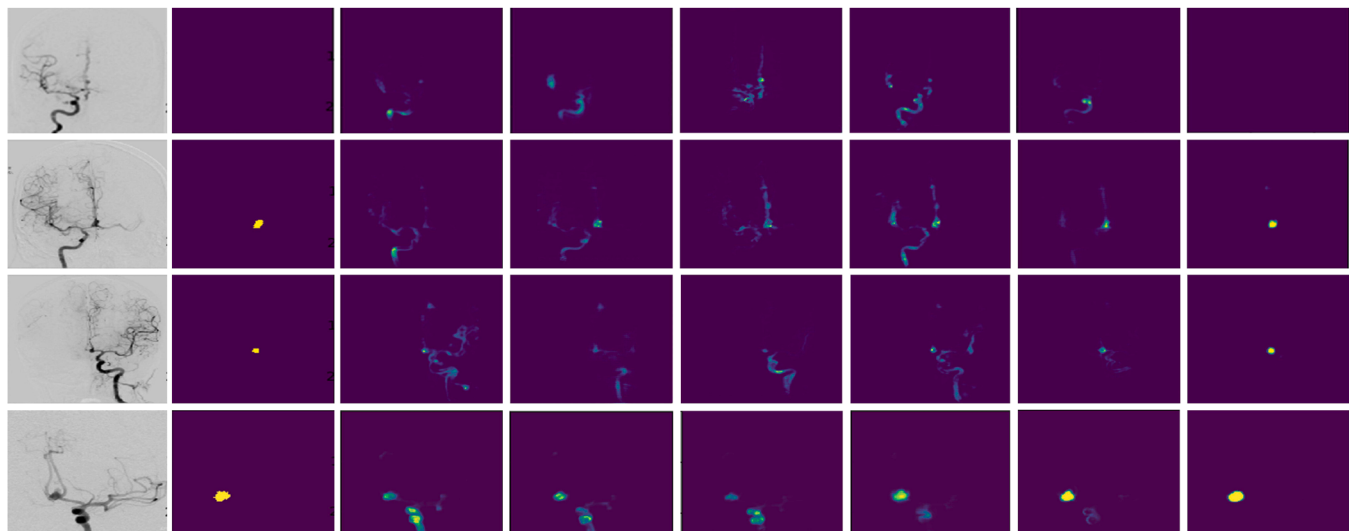


**Fig. 5.** Visual representation of features maps using various formulation sets including proposed CNN architecture.

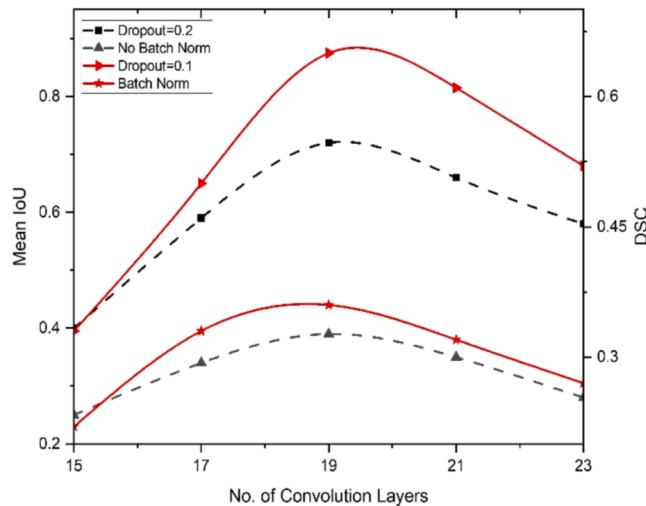


**Fig. 6.** The impact of varying convolutions layers, batch normalization, and dropout on mean IoU and DSC score.

alternative approach for various computer vision tasks. However, in this study, we did not investigate ViTs for several reasons. Firstly, as discussed in the original paper by Dosovitskiy et al. (2020), ViTs heavily rely on large datasets, whereas the ImageNet-1k dataset used in this study is considered a medium-sized dataset. Compared to Convolutional Neural Networks (CNNs), ViTs lack inductive biases for processing images, which requires a larger amount of data for training (Vaswani et al., 2017). In contrast, CNNs process images enabling them to achieve better results with smaller datasets.

In this section, we present a comparison of the segmentation performance of the proposed network with existing state-of-the-art methods, utilizing our DSA image dataset. In addition to segmentation metrics, global accuracy and mean accuracy are also employed. Global accuracy is defined as the ratio of correctly classified pixels to the total number of pixels. Mean accuracy is calculated as the total number of correctly classified pixels over all the pixels. The segmentation models evaluated in this study include FCN (Chen et al., 2020a), PSPNet (Zhao et al., 2017), U-Net (Ronneberger et al., 2015), and SegNet (Badrinarayanan et al., 2017). The overall performance of each method is illustrated in Table 5 and the visual results are depicted in Fig. 7. Among the state-of-the-art methods, U-Net demonstrated the best performance on global accuracy, mean accuracy, mean IoU, and DSC for aneurysm segmentation. SegNet and PSPNet exhibited the second and third best performance, respectively. FCN demonstrated moderate performance in comparison to the other methods. Conversely, the proposed method outperformed all of the state-of-the-art methods on these metrics.

#### 4.5. Evaluation of the proposed method on public medical imaging segmentation datasets

In order to assess the generalizability of the proposed method for aneurysm segmentation, two publicly available datasets, namely ISIC-

2017 and Retina DRIVE ((Mou et al., 2019)), were used for performance evaluation. The ISIC-2017 dataset contains 2000 training images and 300 validation images, while the DRIVE dataset consists of 20 training images and 20 testing images. In order to avoid overfitting on the DRIVE dataset, augmentation techniques were employed to generate 200 training images. For performance comparison on the ISIC-2017 dataset, the latest works including Liu et al. (2022), Li et al. (2020), and Wang et al. (2021) were considered, while for the DRIVE dataset, our results were compared with those of Mishra et al. (2022), Mou et al. (2019), and Tan et al. (2022). The evaluation metrics used include the area under curve (AUC), ACC, Jaccard index (JAC), specificity (SP), and sensitivity (SE). The overall performance of the proposed.

method, as compared to existing methods on the ISIC-2017 and DRIVE datasets, is presented in Tables 6 and 7, respectively. The best performance on the ISIC- 2017 dataset was observed for Liu et al. (2022), achieving overall scores of 85.04 %, 96.30 %, 98.90 %, and 87.99 % for mean IoU, accuracy, SP, and SE, respectively. However, when comparing against the DRIVE dataset, our method achieved comparable performance to the state-of-the-art, demonstrating the generalizability of the proposed system to other domains in medical image analysis.

#### 4.6. Evaluation of blood flow patterns

In order to assess the impact of the proposed 2D finite element model on the overall performance of the rupture prediction framework, we conducted an ablation study. The visualization of shear pressure is illustrated in Fig. 8. The aim of this study is to determine the importance

**Table 4**

Average meanIoU, pixel accuracy, and DSC score for DSA images.

Input	Average Mean IoU	Average Pixel Accuracy	Average DSC
128 × 128	0.78	92.78	0.74
256 × 256	0.81	84.54	0.77
512 × 512	0.76	91.21	0.70

**Table 5**

Evaluation of proposed method for DSA images on various set of experiments.

Test	Batch Training Size	A (%)	P (%)	R (%)	F1 (%)
Test 1	8	512	79.2	75.6	72.6
		256	80.9	77.3	73.1
		128	77.4	76.5	74.6
Test 2	16	512	84.3	81.2	79.9
		256	87.2	84.4	81.0
		128	84.4	82.0	79.9
Test 3	24	512	78.6	76.2	75.6
		256	78.2	75.5	74.9
		128	76.3	75.2	75.1
Test 4	32	512	72.6	70.1	68.3
		256	70.2	69.3	68.3
		128	68.2	65.2	66.4

**Table 3**

Various formulations of proposed segmentation architecture.

Formulation	Encoder side features				Bottom features	Decoder side features				Strides	Dropout	Loss
	L1	L2	L3	L4		L6	L7	L8	L9			
Formulation 1	128	256	512	1024	2028	1024	512	256	128	2 0	0.2	MSE
Formulation 2	64	128	256	512	1024	512	256	128	64	1	0.1	
Formulation 3	32	64	128	256	512	256	128	64	32	2	0.2	MAE
Formulation 4	16	32	64	128	256	128	64	32	16	0	0.1	
Formulation 5	32	64	128	256	512	256	128	64	32	2	0.2	BCE
Proposed method	16	32	64	128	256	128	64	32	16	0	0.1	

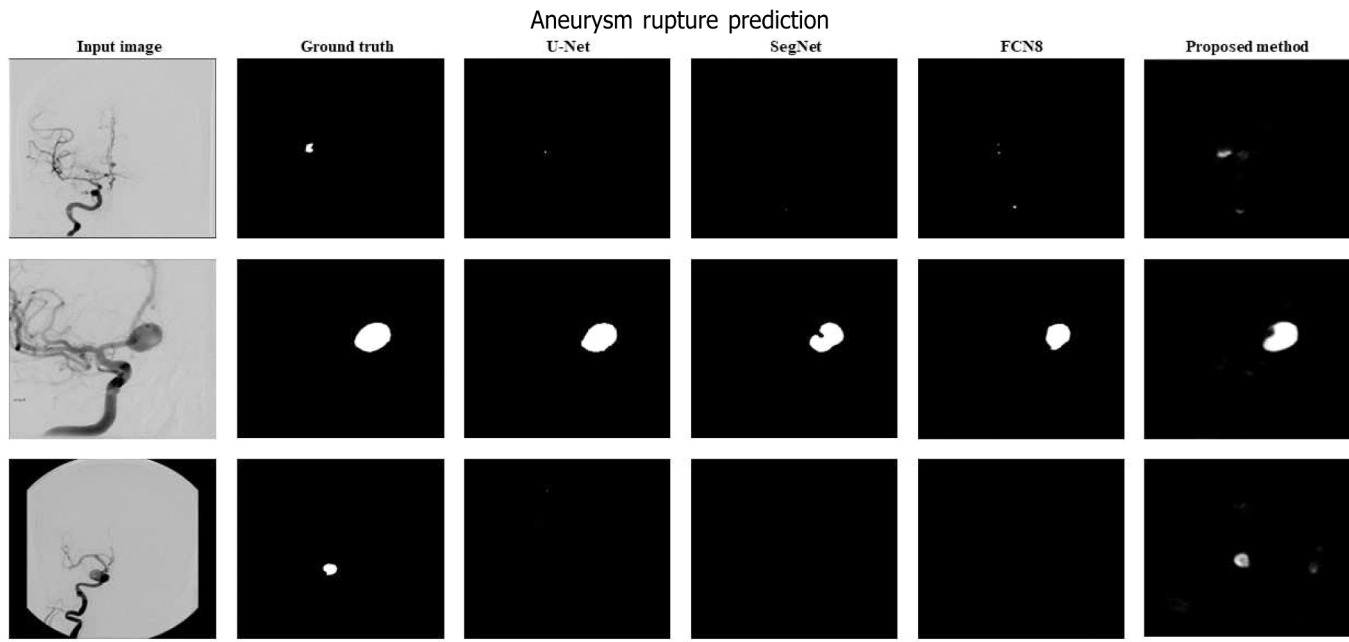


**Fig. 7.** Comparison of the proposed method with state-of-the-art segmentation models using DSA images. The first column displays the input DSA image, the second column displays the ground mask, and the subsequent columns show the predicted mask for each method.

**Table 6**  
Comparison of the proposed method with existing segmentation methods using DSA images.

Method	Global accuracy	Mean accuracy	Mean IoU	DSC
(Long et al., 2014)	0.71	0.73	0.73	0.72
(Zhao et al., 2017)	0.73	0.72	0.73	0.75
(Ronneberger et al., 2015)	0.76	0.77	0.78	0.77
(Badrinarayanan et al., 2017)	0.74	0.73	0.74	0.75
Proposed Method	0.80	0.80	0.81	0.79

**Table 7**  
Segmentation evaluation with state-of-the-art methods using ISIC-2017 dataset.

Method	JAC (%)	ACC (%)	SP (%)	SE (%)
(Liu et al., 2022)	85.04	96.30	98.90	87.99
(Li et al., 2020)	78.10	94.10	96.80	81.20
(Wang et al., 2021)	NA	95.10	93.20	83.50
Proposed Method	<b>80.07</b>	<b>93.25</b>	<b>94.54</b>	<b>84.24</b>

of blood flow patterns in predicting aneurysm rupture risk and to assess the improvement in model performance achieved by including this feature. As shown in Table 9 that the feature set with blood flow patterns generally has higher values for specificity, sensitivity, and AUC compared to the feature set without blood flow patterns. Specifically, the feature set with blood flow patterns has a higher specificity and sensitivity by 0.05–0.07, and a higher AUC of 0.07, suggesting that the addition of blood flow patterns as a feature result in a more accurate and informative classifier for predicting aneurysm risk. Based on Table 9, it is clear that the inclusion of blood flow patterns as a feature significantly.

improves the performance of the aneurysm rupture risk prediction. This indicates that an accurate assessment of sheer pressure on the aneurysm's wall plays an important role in predicting aneurysm rupture risk. Further research in this area is necessary to fully understand the potential benefits and limitations of using blood flow patterns as a

feature in the model. By including more advanced information about blood flow, the proposed StrokeNet framework may predict the likelihood of rupture and provide more accurate risk assessments.

#### 4.7. Performance evaluation of FCBF with other features selection methods

In this section, we evaluated the performance of FCBF with other existing features selection methods. As shown in Table 10, the FCBF method demonstrates good performance specifically with the Decision Tree classifier compared to other feature selection methods and classifiers due to a few key reasons. FCBF selects features based on their correlation with the target variable, aligning with Decision Trees' ability to capture and utilize such correlations, resulting in improved performance. However, other methods like PCA and LASSO regression do not perform well because PCA focuses on capturing the most significant variation in the data, which may not prioritize features highly correlated with the target. Similarly, LASSO regression uses regularization to shrink less relevant features towards zero, which may not effectively capture the specific correlations FCBF identifies. This mismatch between the feature selection approaches of PCA and LASSO regression and the requirements of the Decision Tree classifier may lead to suboptimal performance with those methods.

#### 4.8. Evaluation of various view/slices of aneurysm

In the first set of experiments, we evaluated the performance of our model using only the best view of the aneurysm as selected by the neurosurgeons. This is a common approach in medical imaging studies, where experts manually select the most informative view(s) to minimize variability and bias in the analysis. In the second set of experiments, we excluded the best view selected by the neurosurgeons and used other views where the aneurysm was not as clearly visible in the 2D-DSA images. This set of experiments aimed to evaluate the robustness of our model to the selection of views and to assess whether the performance could be improved by including multiple views. Overall performance of including and excluding best of aneurysm is shown in Table 11.

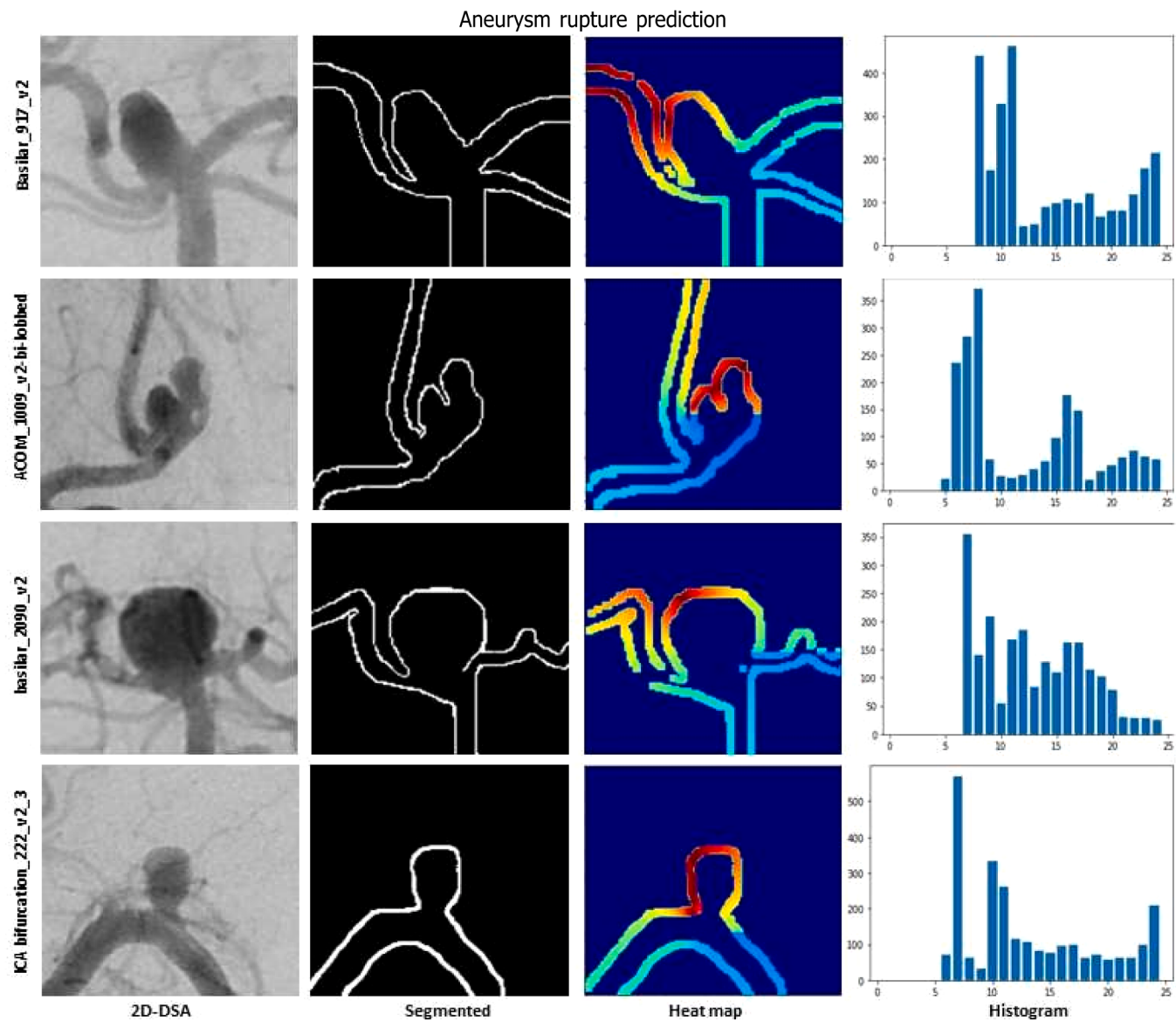


**Fig. 8.** Visualization of blood flow pattern model. The first column displays the input DSA image, followed by the segmented aneurysm in the second column. The third column demonstrates the stress exerted by the blood on the wall of the aneurysm. The fourth column showcases the histogram of the distance from the center of the aneurysm.

**Table 8**

Comparison of the proposed and existing methods for segmentation using DRIVE dataset.

Method	AUC (%)	ACC (%)	SP (%)	SE (%)
(Mishra et al., 2022)	98.74	94.80	98.07	74.06
(Mou et al., 2019)	97.96	95.94	97.88	81.26
(Tan et al., 2022)	96.15	95.14	97.40	75.45
Proposed Method	94.02	93.12	94.01	73.21

#### 4.9. Analysis of various features set for aneurysm rupture classification

To extract information from the masks of the aneurysms, geometric and deep features, blood flow patterns, as well as Fourier descriptors were obtained for all segmented aneurysms. Two distinct types of images were utilized in the feature extraction process. The original DSA was used to extract deep features, while a binary mask was used to extract first-order features. The first-order features include blood flow

**Table 9**

Impact of blood flow pattern for different classes of patients.

Aneurysm	With blood flow			Without blood flow		
	SP	SE	AUC	SP	SE	AUC
Mild	0.86	0.67	0.76	0.79	0.60	0.69
Moderate	0.88	0.71	0.80	0.81	0.64	0.73
Severe	0.90	0.77	0.84	0.83	0.70	0.77
Critical	0.93	0.81	0.88	0.86	0.74	0.81

pattern, Fourier descriptor, and geometrical features (7 features), whereas the DSA images were used to estimate 2048 features using Inception-v3 model. The parameters from the training samples were utilized to normalize the testing samples after normalizing the training data to zero mean and one standard deviation (std) for each feature selection using correlation-based filter (FCBF) was used to determine the key factors that were helpful in rupture classification. After separately selecting the image features and vesselness features, we obtained seven geometrical features, blood flow patterns, and deep features. The

**Table 10**

Evaluation of FCBF with existing features reductions methods.

Classifier	FCBF				PCA				LASSO Regression			
	ACC	P	R	F1	ACC	P	R	F1	ACC	P	R	F1
Decision Tree	0.85	0.82	0.84	0.83	0.82	0.79	0.81	0.80	0.83	0.83	0.79	0.78
SVM	0.78	0.77	0.76	0.78	0.77	0.76	0.75	0.76	0.79	0.81	0.79	0.78
MLP	0.78	0.79	0.75	0.75	0.81	0.76	0.80	0.79	0.82	0.79	0.76	0.77

**Table 11**

Performance Evaluation of the Proposed Method Using Best View and Excluded Best View in Aneurysm Risk Analysis.

Model	ACC	SE	SP
Best View	0.90	0.85	0.89
Excluded Best View	0.82	0.78	0.84

hyperparameter was determined to be 0.0275 using a set of various cross-validation methods. It is noteworthy that 7 shape and first-order features have been chosen, which implies that there are differences among various aneurysm classes in terms of shape and image intensity i.e., Mild, Moderate, Severe, and Critical. An aneurysm's size, for instance, can be represented by its "major axis length." Elongation, sphericity, and aspect ratio are indicators of how smooth a shape is in comparison to its shape. These traits differentiate aneurysm classes visible in.

images but challenging to quantify without automated processing.

We compared Decision Tree with six classifiers using selected feature sets and conducted k-fold cross-validation using the 2D-DSA training dataset. In the SVM classifier, a grid parameter was used where the gamma parameter for the RBF kernel varied from 0.1 to 0.001, and the C parameter ranged between 0.1 and 10. Finally,  $C=1$  and  $\text{gamma}=0.02$  were chosen as the ideal model parameters. The purpose of tuning hyperparameters and conducting cross-validation is to improve the performance of the classifier on unseen data. By finding the best combination of hyperparameters through cross-validation, we can increase the generalization ability of the classifier and avoid overfitting to the training data. For all other classifiers, the hyperparameters for various cross-fold validation are given in Table 12. The mean ROC curves for training data are shown in Fig. 9. As shown in Fig. 9, Decision Tree and SVM both have close performance on the train data however, on test set as shown in Fig. 10, Decision Tree outperformed all other classifiers including SVM. In addition, we assess the effectiveness of the proposed method for aneurysm rupture prediction by producing mean ROC curves for each aneurysm class using the Decision Tree classifier, which is displayed in Fig. 11.

To investigate the potential usefulness of different feature sets for

**Table 12**

Hyperparameter setting for various classifiers.

Classifier	Parameter	No. Cross fold	Best cross-fold
Decision Tree	Max-depth, max-leaf node	8	65 max-depth
Logistic Regression	Solver, penalty, C	5	C:0.01, penalty:l2, solver: liblinear
KNN	N-neighbour, metric,	9	metric:manhattan, n- neighbour:13, weights: uniform
SVM	Kernels, C	6	C:1.0, gamma:scale, kernel: rbf
MLP	Activation, alpha, hidden-layersize, learning-rate, solver	9	activation:relu, alpha:0.001, hidden-layersize:33, learning-rate:constt, solver:adam
AdaBoost	n-estimator	5	n-estimator:150

ROC of various classifiers on Aneurysm Training Set

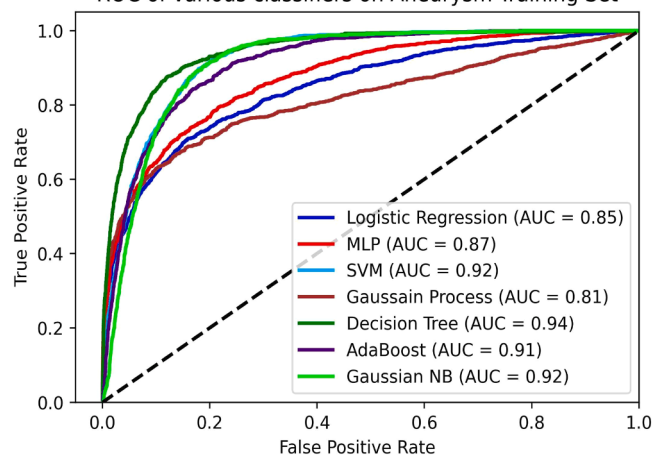


Fig. 9. Mean ROC curves of various classifiers for aneurysm criticality classification on validation set during training. A comparison of Decision Tree with other set of classifiers for aneurysm rupture prediction.

ROC of various classifiers on Aneurysm Testing Set

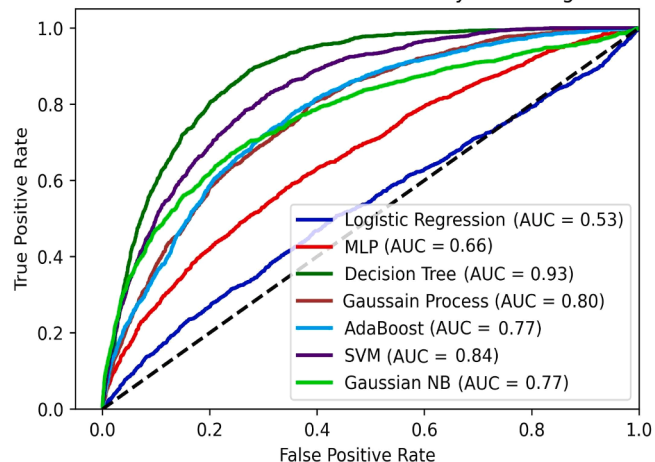
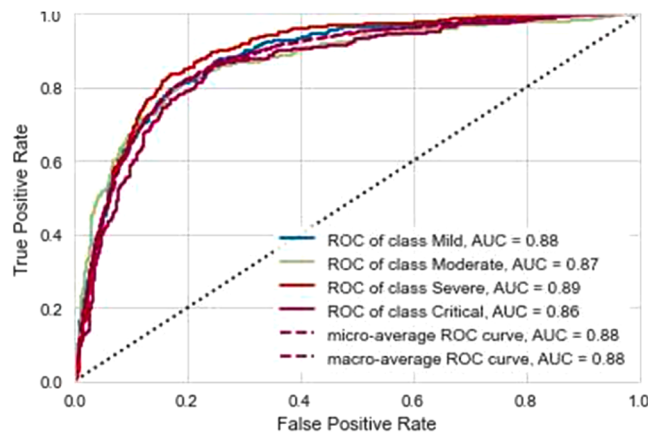


Fig. 10. The mean ROC curves generated to compare the performance of Decision Tree with other classifiers for predicting aneurysm criticality on a test set.

classifying aneurysm criticality, we conducted experiments using Decision Tree with various feature sets. These experiments involved training models using deep features, geometrical features, Fourier descriptors, blood flow patterns, and a combination of all these feature sets. Fig. 11 displays the ROC curves for the testing samples, showing that the classifier is more confident when all features are combined compared to individual.

feature sets. The sensitivities for specificity were 0.86 and 0.89, respectively. From the Fig. 12, it is evident that individual feature sets, especially Fourier descriptors and blood flow patterns, are not sufficient for analyzing aneurysm rupture criticality compared to geometrical features and deep features. Although the Decision Tree classifier with



**Fig. 11.** The performance of the Decision Tree across different classes of aneurysms is assessed using ROC curves to determine the effectiveness of the proposed pipeline for aneurysmal criticality analysis.

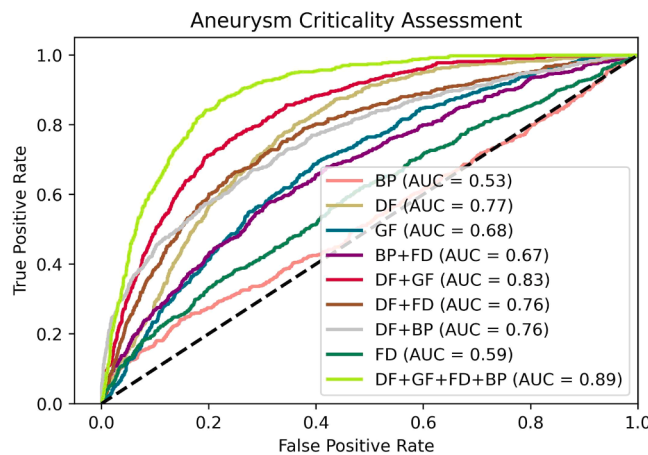


**Fig. 12.** Performance evaluation of proposed pipeline using individual and fusion of different features. GF = geometrical features, DF = deep learning, BF = blood flow pattern, and FD = Fourier descriptor.

combined features performed better than individual feature sets, an improvement in AUC by 0.06 was observed when all features were fused together compared to the best AUC score of 0.83 obtained with deep features and geometrical features. Overall, the fusion of all features yielded noticeable improvement.

To summarize, our study employed segmented aneurysm masks to extract geometrical features, blood flow patterns, and Fourier descriptors along with deep features extracted from original DSA images to analyze the aneurysm criticality. We compared various classifiers and feature sets and found that deep features along with other first-order features could help the neurosurgeon to effectively analyze the aneurysm criticality. A similar study is also conducted by Wu et al. (2022) to find ruptured and unruptured aneurysms using radiomics and deep features (features extracted via ResNet50).

## 5. Discussion

The aim of this study is to assess the viability and efficacy of the proposed pipeline for detecting, segmenting, and classifying aneurysms based on 2D-DSA images. The pipeline is built using a combination of first-order, geometrical, blood flow, and deep features. To address the issue of identifying the criticality of an unruptured aneurysm, we merged mentioned features and employed a Decision Tree classifier. Furthermore, to enhance the usage of image information such as shape

and vasculature, we generated a vesselness feature map for each image (segmented mask and DSA image). This enabled the classifier to incorporate both image and vesselness information as multi-channel inputs.

This pipeline, serving as a predictor of aneurysm rupture risk, has the potential to be seamlessly integrated with other aneurysm risk analysis techniques, thereby enhancing the early-stage diagnosis of patients. For instance, Malik et al. (2023) developed a framework for determining the criticality of an aneurysm rupture, known as the Aneurysm Rupture Criticality Prediction (ARCP) score. This score quantifies the relative probabilities of aneurysmal rupture over the life-time (ARCP-lifetime) and within a five-year period (ARCP- 5 yrs). The framework employs association rule mining and machine learning techniques to identify combinations of risk factors, extracted from clinical notes, that are commonly associated with subarachnoid hemorrhage. The outcomes of StrokeNet will be integrated into ARCP framework Malik et al. (2023) to enhance the reliability of the earlier developed score.

Having a good understanding of the role that geometric features play in deep learning is crucial when it comes to distinguishing aneurysms from surrounding vasculatures. One example of this is the use of mesh CNN, which was trained to differentiate between aneurysms and arteries by utilizing triangular surface meshes generated from Time-of-Flight (TOF) MRA data. According to a study by Timmins et al. (2022), MRA had a lower false positiverate compared to DSA. It had an average sensitivity of 65 % and an average of 1.8 false positives per scan. Another study conducted by Zhou et al. (2019) used a transferable multi-model ensemble (MMEN) architecture to identify aneurysms by analyzing 3D cerebrovascular mesh models obtained from vasculature structures. The detection models were trained using various local and global geometric properties, including the Gaussian curvature, form diameter function, and wave kernel signature (WKS). The algorithm achieved a sensitivity of 94.8 %, an F1 score of 94.7 %, and an accuracy of 95.1 %. These studies.

demonstrate the importance of incorporating geometric features and deep features to detect aneurysms. By utilizing various geometric properties, such as curvature and diameter, these models can achieve high levels of accuracy and sensitivity. This information can prove to be useful in developing more effective detection and diagnosis methods for aneurysms, which can ultimately improve patient outcomes.

Bizjak et al. (2020) employed point clouds to represent the surfaces of arteries and aneurysms, using graph convolutions to recognize the patches unique to aneurysms. Wu et al. (2022) utilized deep features and radiomics traits to evaluate ruptured and unruptured aneurysms based on CTA images. Consequently, it is reasonable to propose networks for aneurysm identification and classification, utilizing image-based features, geometric characteristics, and shape-based convolution, in addition to CFD-based features. The vasculature-based feature maps provide a further explanation for classification and rupture analysis. However, deep learning approaches that incorporate shape features with vascular aspects have not yet been fully explored in medical image analysis.

Moreover, on a dataset consisting of 35 individuals with aneurysms, we used our study to assess the effectiveness of our blood flow model. To evaluate the accuracy of the model, we evaluated the model against expert evaluation. For each patient, the aneurysm boundary was separated into three distinct areas as.

shown in Fig. 13 based on the blood shear This categorization allowed us to assess the model's pressure on the aneurysm wall: High, Medium, and Low. performance in predicting blood flow patterns accurately. Our findings indicated that the model exhibited promising results in highlighting High, Medium, and Low blood flow regions, predicting 28 out of a total of 35 for High, 27 for Medium, and 22 for Low shear pressure regions, respectively. The confusion matrix for each region is presented in Fig. 14. We also noticed that the model's accuracy in terms of shear pressure on the aneurysm wall located at the basilar tip and ICA bifurcation is more accurately detected by the model compared to other locations such as the Anterior Communicating Artery and Internal Carotid Artery. The results demonstrate the potential for

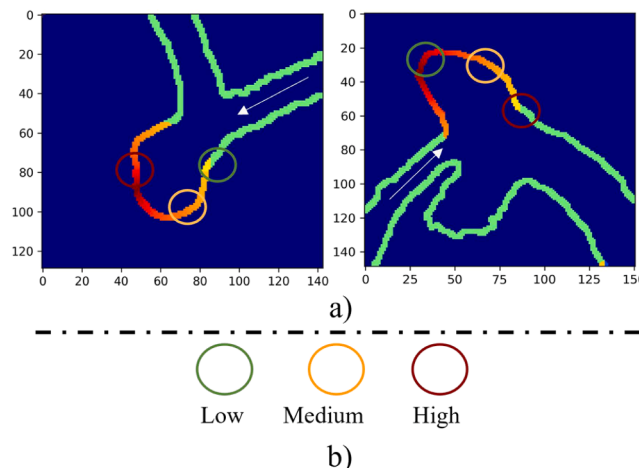


**Fig. 13.** Illustration of high shear pressure on the wall of the aneurysm using heatmap where a) shows the heatmap and neurosurgeons identified regions of high shear pressure and b) shows the annotation used by neurosurgeons. Circles indicate expert annotation of the high shear pressure according to the flow of blood in the associated artery indicated by the white arrow.

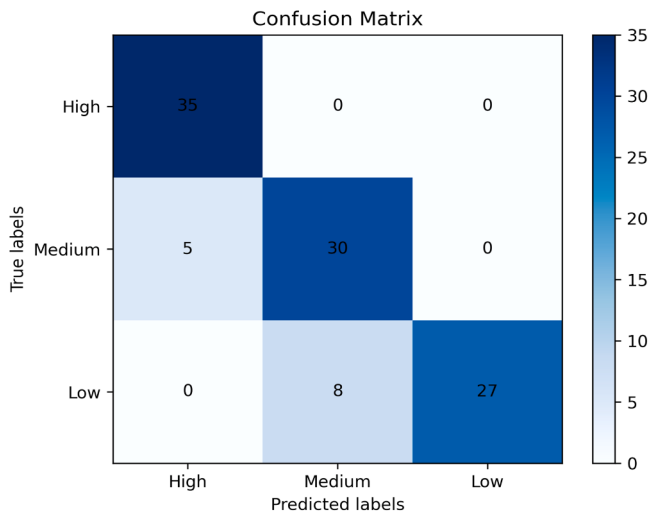


**Fig. 14.** Confusion matrix of blood flow pattern in contrast to expert annotation.

accurately underlining the sheer pressure in the aneurysm wall. However, it is important to note that the blood flow within aneurysms is a highly complex and dynamic phenomenon influenced by numerous factors, including the aneurysm's shape, size, and location, as well as the properties of the blood itself. By expanding the concept of obtaining features specific to blood flow patterns in aneurysms, future research can potentially enhance the accuracy of risk estimation for aneurysm rupture. This, in turn, could contribute to more effective treatment planning and improved patient outcomes.

Besides the aneurysm criticality analysis, in this study, we also evaluated the proposed aneurysm segmentation part and other existing state-of-the-art methods. Our quantitative analysis shows that SegNet performed poorly as compared to the other evaluated segmentation models. The nature of the model allows the network to train on pixel-to-pixel segmentation, which seems to be effective in case of a large dataset and natural outdoor scenes. However, in case of medical image analysis, down-sampling of the SegNet method produces poor features maps for aneurysm segmentation, letting network focus on large regions of interest and ignore small regions of interest, resulting in poor performance. In addition, large end-to-end models such as FCN and U-Net

doesn't work well on small datasets, leading to an under fitting problem. In addition, U-Net also showed the same trends as FCN, for instance, when the layers are reduced to 23 convolutions, and 2.6 million parameters, the model is not able to sufficiently perform on data with complex patterns. In the proposed study, we reduced the total number of convolutional layers to 19, total parameters to 1.9 million, and the number of feature maps to 512 at the bottom of the network in order to find a good fit for the given data. The impact of varying convolution layers, batch normalization, and dropout, on mean IoU and DSC is illustrated in Fig. 6.

To summarize, the proposed pipeline is able to analyze aneurysm rupture criticality. Further, the obtained results also confirm the AUC curve on the Decision Tree (0.88–0.93) which is better than Wu et al. (2022) (AUC=0.91 for 1205 train and 303 test set) and Shi et al. (2020) (AUC=0.82 for 400 train and 100 test set) where they used CTA images and SVM as a classifier. Still, such a pipeline could serve as a significant tool to analyze aneurysm screening at initial screening, however, performance improvement is still needed for automated decision-making.

### 5.1. Limitations

Despite the impact of the proposed system for segmentation and rupture risk prediction of the aneurysm, there are certain limitations. Addition to deep and geometrical features, our recent work indicate several other factors that are associated with aneurysm rupture such as patient family history, smoking, age, sex, and hypertension (Malik et al., 2023). In our future studies, we aim to combine the pipeline of Natural Language Processing on clinical notes, with StrokeNet to improve our proposed aneurysm rupture score prediction. Secondly, the system is robust in segmenting the aneurysm regions but for some aneurysms, boundaries are not segmented efficiently. As a result, pre-processing is used to center crop the image and to accurately extract aneurysm boundaries. Moreover, during experimental evaluation, some loops were also detected as aneurysms. A possible reason for the misdetection could be the scarcity in the dataset where the network is unable to completely differentiate between loops and aneurysms. In addition to the above-mentioned limitations, other limitations include consideration of Newtonian effect of blood in the blood flow model. In aneurysms, where the flow of blood is highly turbulent and the geometry is irregular, the Newtonian assumption can lead to inaccurate predictions of hemodynamic parameters such as wall stress and flow velocity. Non-Newtonian effects can play an important role in these situations, as they can influence the flow patterns and the distribution of hemodynamic forces on the aneurysm wall. Although blood is a non-Newtonian fluid, our model assumes blood flow to be Newtonian. While this assumption simplifies the computational complexity of our model, it may not accurately capture the flow behavior of blood in certain situations, such as in areas of high shear stress or in regions with complex geometries. Non-Newtonian effects can play an important role in these situations, as they can influence the flow patterns and the distribution of hemodynamic forces on the aneurysm wall. Therefore, our model's predictions may not be entirely representative of the true hemodynamic conditions in aneurysms, especially in regions with complex geometry or high stress. Moreover, the model of blood flow is also dependent on the performance of the segmentation. During the experiments, we also noticed that besides the aneurysm wall, some adjacent arteries were also segmented that further limiting the performance of the blood flow model.

### 6. Conclusion

This article presents a novel and generalizable approach for aneurysm segmentation and the prediction of its rupture risk. To our knowledge, this is the first study that utilizes 2D-DSA images to compute geometrical features, deep features, Fourier descriptors, and

blood flow patterns for the analysis of aneurysmal rupture criticality. We fused distinct feature sets, applied the fast correlation-based filter for feature selection, and used a decision tree classifier. The final results were compared with a set of expert-annotated patient DSA images. Additionally, we proposed a customized end-to-end CNN.

model for aneurysm segmentation and compared the results with existing state-of-the-art methods. For the aneurysm rupture prediction, we annotated a total of 297 patients and categorized them into four classes: Mild, Moderate, Severe, and Critical. We extracted different features, including deep feature, geometrical features, Fourier descriptor and blood flow patterns, to analyze aneurysm criticality. We achieved an overall accuracy of 85 % for a total of 69 patients in the test set. Furthermore, our results suggest that, in addition to other significant features, the neck diameter, size ratio, and aspect ratio of the aneurysm play a crucial role in rupture criticality analysis. For the segmentation evaluation, we achieved an average of 0.81, 0.94, and 0.87 for mean IoU, pixel, and detection accuracy, respectively. Additionally, to evaluate the generalizability of our approach for segmentation, we used publicly available datasets, including ISIC-2017 and DRIVE, and compared the performance of our method with existing methods. The results indicate that our proposed method is generalizable for segmentation problems in other medical image analysis domains. Finally, we comparatively evaluated the performance of a single and fusion of different features for aneurysm risk prediction and achieved an overall score of 85 % accuracy on the fusion of deep, geometrical, Fourier descriptor, and blood flow pattern features. For future work, we aim to simplify the framework into a single CNN network for both segmentation and rupture prediction tasks. We also plan to develop a 5-year rupture and growth score using multimodal data.

#### CRediT authorship contribution statement

**Muhammad Irfan:** Methodology, Software, Validation, Formal analysis, Investigation, Visualization, Writing - original draft. **Khalid Mahmood Malik:** Resources, Supervision, Conceptualization, Funding acquisition, Project administration, Validation, Writing - review & editing. **Jamil Ahmad:** Software, Methodology, Writing - review & editing. **Ghaus Malik:** Data curation, Resources.

#### Declaration of Competing Interest

The authors declare that they have no known competing financial interests or personal relationships that could have appeared to influence the work reported in this paper.

#### Data availability

The data that has been used is confidential.

#### Acknowledgements

This work is supported by Brain Aneurysm Foundation USA. We also deeply acknowledge the administrative and technical support of Henry Ford Health System, MI.

#### References

- Ajiboye, N., Chalouhi, N., Starke, R.M., Zanaty, M., Bell, R., 2015. Unruptured cerebral aneurysms: evaluation and management. *Sci. World J.* 2015.
- An, X., He, J., Di, Y., Wang, M., Luo, B., Huang, Y., Ming, D., 2022. Intracranial aneurysm rupture risk estimation with multidimensional feature fusion. *Front. Neurosci.* 16.
- Badrinarayanan, V., Kendall, A., Cipolla, R., 2017. Segnet: a deep convolutional encoder-decoder architecture for image segmentation. *IEEE Trans. Pattern Anal. Mach. Intell.* 39 (12), 2481–2495.
- BAF Statistics. Statistics and Facts. (<https://www.bafound.org/statistics-and-facts/>). (Accessed 19 June 2023.). 2023.
- Ž. Bizjak, B. Likar, F. Pernuš, Ž. Špiclin. Vascular surface segmentation for intracranial aneurysm isolation and quantification. In: Proceedings of the Twenty Third International Conference, Medical Image Computing and Computer Assisted Intervention—MICCAI 2020, Springer, Lima, Peru, October 4–8, 2020, Part VI 23, 128–137.
- Bogunović, H., Pozo, J.M., Villa-Uriol, M.C., Majoe, C.B., van den Berg, R., Gratama van Andel, H.A., Macho, J.M., Blasco, J., San Román, L., Frangi, A.F., 2011. Automated segmentation of cerebral vasculature with aneurysms in 3dra and tof-mra using geodesic active regions: an evaluation study. *Med. Phys.* 38 (1), 210–222.
- Brinjikji, W., Kallmes, D.F., Cloft, H.J., Lanzino, G., 2016. Age-related outcomes following intracranial aneurysm treatment with the pipeline embolization device: a subgroup analysis of the intrepid registry. *J. Neurosurg.* 124 (6), 1726–1730.
- Cebral, J.R., Mut, F., Weir, J., Putman, C.M., 2011. Association of hemodynamic characteristics and cerebral aneurysm rupture. *Am. J. Neuroradiol.* 32 (2), 264–270.
- Chen, G., Wei, X., Lei, H., Liqin, Y., Yuxin, L., Yakang, D., Daoying, G., 2020a. Automated computer-assisted detection system for cerebral aneurysms in time-of-flight magnetic resonance angiography using fully convolutional network. *Biomed. Eng. OnLine* 19 (1), 1–10.
- Chen, Y., Courbebaisse, G., Yu, J., Lu, D., Ge, F., 2020b. A method for giant aneurysm segmentation using euler's elastica. *Biomed. Signal Process. Control* 62, 102111.
- Dai, X., Huang, L., Qian, Y., Xia, S., Chong, W., Liu, J., Di Ieva, A., Hou, X., Ou, C., 2020. Deep learning for automated cerebral aneurysm detection on computed tomography images. *Int. J. Comput. Assist. Radiol. Surg.* 15 (4), 715–723.
- Dakua, S.P., Abinahed, J., Al-Ansari, A., 2018. A pca-based approach for brain aneurysm segmentation. *Multidimens. Syst. Signal Process.* 29 (1), 257–277.
- A. Dosovitskiy, L. Beyer, A. Kolesnikov, D. Weissenborn, X. Zhai, T. Unterthiner, M. Dehghani, M. Minderer, G. Heigold, S. Gelly, et al. An image is worth 16×16 words: transformers for image recognition at scale. arXiv preprint arXiv:2010.11929, 2020.
- Feghali, J., Gami, A., Xu, R., Jackson, C.M., Tamargo, R.J., McDougall, C.G., Huang, J., Caplan, J.M., 2021. Application of unruptured aneurysm scoring systems to a cohort of ruptured aneurysms: are we underestimating rupture risk? *Neurosurg. Rev.* 44 (6), 3487–3498.
- Gan, J., Peng, Z., Zhu, X., Hu, R., Ma, J., Wu, G., 2021. Brain functional connectivity analysis based on multi-graph fusion. *Med. Image Anal.* 71, 102057.
- Ivantits, M., Goubergrits, L., Kuhnigk, J.-M., Huellebrand, M., Bruening, J., Kossen, T., Pfahring, B., Schaller, J., Spuler, A., Kuehne, T., et al., 2022. Detection and analysis of cerebral aneurysms based on x-ray rotational angiography—the cada 2020 challenge. *Med. Image Anal.* 77, 102333.
- Janiga, G., Berg, P., Sugiyama, S., Kono, K., Steinman, D., 2015. The computational fluid dynamics rupture challenge 2013—phase i: prediction of rupture status in intracranial aneurysms. *Am. J. Neuroradiol.* 36 (3), 530–536.
- T. Jerman, F. Pernuš, B. Likar, Ž. Špiclin. Aneurysm detection in 3d cerebral angiograms based on intra-vascular distance mapping and convolutional neural networks. In: Proceedings of the Fourteenth International Symposium on Biomedical Imaging (ISBI 2017), IEEE, 612–615, 2017.
- Jerman, T., Chien, A., Pernuš, F., Likar, B., Špiclin, Ž., 2019. Automated cutting plane positioning for intracranial aneurysm quantification. *IEEE Trans. Biomed. Eng.* 67 (2), 577–587.
- Kleinloog, R., De Mul, N., Verweij, B.H., Post, J.A., Rinkel, G.J., Ruigrok, Y.M., 2018. Risk factors for intracranial aneurysm rupture: a systematic review. *Neurosurgery* 82 (4), 431–440.
- Labhane, Gaurav, et al., 2020. Detection of pediatric pneumonia from chest X-ray images using CNN and transfer learning. In: *3rd international conference on emerging technologies in computer engineering: machine learning and internet of things (ICETE)*. IEEE.
- Li, X., Yu, L., Chen, H., Fu, C.-W., Xing, L., Heng, P.-A., 2020. Transformation-consistent self-ensembling model for semisupervised medical image segmentation. *IEEE Trans. Neural Netw. Learn. Syst.* 32 (2), 523–534.
- Liu, Y., Zhou, J., Liu, L., Zhan, Z., Hu, Y., Fu, Y., Duan, H., 2022. Fcp- net: a feature-compression-pyramid network guided by game-theoretic interactions for medical image segmentation. *IEEE Trans. Med. Imaging* 41 (6), 1482–1496.
- J. Long, E. Shelhamer, T. Darrell. Fully convolutional networks for semantic segmentation. CoRR, abs/1411.4038, 2014. <http://arxiv.org/abs/1411.4038>.
- Malik, K., Anjum, S.M., Soltanian-Zadeh, H., Malik, H., Malik, G.M., 2018. A framework for intracranial saccular aneurysm detection and quantification using morphological analysis of cerebral angiograms. *IEEE Access* 6, 7970–7986.
- Malik, K., Khalid, et al., 2023. Toward grading subarachnoid hemorrhage risk prediction: a machine learning-based aneurysm rupture score. *World Neurosurgery* 172, e19–e38.
- Meng, Cai, et al., 2020. Multiscale dense convolutional neural network for DSA cerebrovascular segmentation. *Neurocomputing* 373, 123–134.
- S. Minaee, Y.Y. Boykov, F. Porikli, A.J. Plaza, N. Kehtarnavaz, D. Terzopoulos. Image segmentation using deep learning: a survey. *IEEE Transactions on Pattern Analysis and Machine Intelligence*, 2021.
- Mishra, S., Zhang, Y., Chen, D.Z., Hu, X.S., 2022. Data-driven deep supervision for medical image segmentation. *IEEE Trans. Med. Imaging*.
- Mou, L., Chen, L., Cheng, J., Gu, Z., Zhao, Y., Liu, J., 2019. Dense dilated network with probability regularized walk for vessel detection. *IEEE Trans. Med. Imaging* 39 (5), 1392–1403.
- Nakao, T., Hanaoka, S., Nomura, Y., Sato, I., Nemoto, M., Miki, S., Maeda, E., Yoshikawa, T., Hayashi, N., Abe, O., 2018. Deep neural network-based computer-assisted detection of cerebral aneurysms in mr angiography. *J. Magn. Reson. Imaging* 47 (4), 948–953.
- A. Nikravanshalmani, M. Karamimohammadi, J. Dehmehki. Segmentation and separation of cerebral aneurysms: a multi-phase approach. In: Proceedings of the Eighth International Symposium on Image and Signal Processing and Analysis (ISPAN), IEEE, 505–510, 2013.

- Park, A., Chute, C., Rajpurkar, P., Lou, J., Ball, R.L., Shpanskaya, K., Jabarkheel, R., Kim, L.H., McKenna, E., Tseng, J., et al., 2019. Deep learning–assisted diagnosis of cerebral aneurysms using the headxnet model. *JAMA Netw. Open* 2 (6), e195600.
- T.R. Patel, N. Palwal, P. Jaiswal, M. Waqas, M. Mokin, A.H. Siddiqui, H. Meng, R. Rai, V. Tutino. Multi-resolution cnn for brain vessel segmentation from cerebrovascular images of intracranial aneurysm: a comparison of u-net and deepmedic. In: Medical Imaging 2020: Computer-Aided Diagnosis, SPIE, 11314, 677–685, 2020.
- Qiu, Y., Wang, J., Zhao, J., Wang, T., Zheng, T., Yuan, D., 2022. Association between blood flow pattern and rupture risk of abdominal aortic aneurysm based on computational fluid dynamics. *Eur. J. Vasc. Endovasc. Surg.* 64 (2–3), 155–164.
- Quinlan, J.R., 2014. C4. 5: Programs for Machine Learning. Elsevier.
- I. Rahmany , N. Khelifa. Detection of intracranial aneurysm in an- giographic images using fuzzy approaches. In: Proceedings of the International Image Processing, Applications and Systems Conference, IEEE, 1–6, 2014.
- Ronneberger, O., Fischer, P., Brox, T., 2015. U-net: Convolutional networks for biomedical image segmentation. In: Proceedings of the International Conference on Medical image computing and computer-assisted intervention. Springer, pp. 234–241.
- Rusak, F., Santa Cruz, R., Lebrat, L., Hlinka, O., Fripp, J., Smith, E., Fookes, C., Bradley, A.P., Bourgeat, P., Initiative, A.D.N., et al., 2022. Quantifiable brain atrophy synthesis for benchmarking of cortical thickness estimation methods. *Med. Image Anal.* 82, 102576.
- Sharif, M., Amin, J., Nisar, M.W., Anjum, M.A., Muhammad, N., Shad, S.A., 2020. A unified patch-based method for brain tumour detection using features fusion. *Cogn. Syst. Res.* 59, 273–286.
- Shi, Z., Miao, C., Schoepf, U.J., Savage, R.H., Dargis, D.M., Pan, C., Chai, X., Li, X.L., Xia, S., Zhang, X., et al., 2020. A clinically applicable deep-learning model for detecting intracranial aneurysm in computed tomography angiography images. *Nat. Commun.* 11 (1), 1–11.
- Sichtermann, T., Faron, A., Sijben, R., Teichert, N., Freiherr, J., Wies- mann, M., 2019. Deep learning–based detection of intracranial aneurysms in 3d tof-mra. *Am. J. Neuroradiol.* 40 (1), 25–32.
- Spanhol, Fabio Alexandre, et al. "Breast cancer histopathological image classification using convolutional neural networks." *2016 international joint conference on neural networks (IJCNN)*. IEEE, 2016.
- Steinman, D.A., Hoi, Y., Fahy, P., Morris, L., Walsh, M.T., Aristokleous, N., Anayiotos, A. S., Papaharilaou, Y., Arzani, A., Shadden, S.C., et al., 2013. Vari- ability of computational fluid dynamics solutions for pressure and flow in a giant aneurysm: the asme 2012 summer bioengineering conference cfd challenge. *J. Biomech. Eng.* 135 (2).
- Stember, J.N., Chang, P., Stember, D.M., Liu, M., Grinband, J., Filippi, C.G., Meyers, P., Jambawalikar, S., 2019. Convolutional neural networks for the detection and measurement of cerebral aneurysms on magnetic resonance angiography. *J. Digit. Imaging* 32 (5), 808–815.
- Stumpo, V., Staartjes, V.E., Espósito, G., Serra, C., Regli, L., Olivi, A., Sturiale, C.L., 2022. Machine learning and intracranial aneurysms: from detection to outcome prediction. In: Proceedings of the Machine Learning in Clinical Neuroscience: Foundations and Applications. Springer, pp. 319–331.
- Tan, Y., Yang, K.-F., Zhao, S.-X., Li, Y.-J., 2022. Retinal vessel segmentation with skeletal prior and contrastive loss. *IEEE Trans. Med. Imaging*.
- Tang, X., Zhou, L., Wen, L., Wu, Q., Leng, X., Xiang, J., Zhang, X., 2022. Morphological and hemodynamic characteristics associated with the rupture of multiple intracranial aneurysms. *Front. Neurol.* 12, 2564.
- K. Timmins, I. van der Schaaf, I. Vos, Y. Ruigrok, B. Velthuis, H. Kuijf. Deep learning with vessel surface meshes for intracranial aneurysm de- tection. In: Proceedings of the Medical Imaging 2022: Computer-Aided Diagnosis, SPIE, 12033, 633–637, 2022.
- Timmins, K.M., van der Schaaf, I.C., Bennink, E., Ruigrok, Y.M., An, X., Baumgartner, M., Bourdon, P., De Feo, R., Di Noto, T., Dubost, F., et al., 2021. Comparing methods of detecting and segmenting unruptured intracra- nial aneurysms on tof-mras: the adam challenge. *Neuroimage* 238, 118216.
- Vaswani, A., Shazeer, N., Parmar, N., Uszkoreit, J., Jones, L., Gomez, A.N., Kaiser, L., Polosukhin, I., 2017. Attention is all you need. *Adv. Neural Inf. Process. Syst.* 30.
- Walther, G., Martin, C., Haase, A., Nestler, U., Schob, S., 2022. Machine learn- ing for rupture risk prediction of intracranial aneurysms: challenging the phases score in geographically constrained areas. *Symmetry* 14 (5), 943.
- Wang, S., Yin, Y., Wang, D., Wang, Y., Jin, Y., 2021. Interpretability-based multimodal convolutional neural networks for skin lesion diagnosis. *IEEE Trans. Cybern.*
- Wang, Xinqi, et al., 2019. An appraisal of lung nodules automatic classification algorithms for CT images. *Sensors* 19 (1), 194.
- Wilson, D.L., Noble, J.A., 1997. Segmentation of cerebral vessels and aneurysms from mr angiography data. In: Preoceedings of the Biennial International Conference on Information Processing in Medical Imaging. Springer, pp. 423–428.
- Wu, D., Gu, Qi, P., Cao, X., Wu, D., Chen, L., Qu, G., Wang, J., Pan, X., Wang, X., et al., 2022. Evaluation of an automated intracranial aneurysm detection and rupture analysis approach using cascade detection and classification networks. *Comput. Med. Imaging Graph.* 102, 102126.
- Xia, C., Xu, B., Nan. Inception-v3 for flower classification. In: Preoceedings of the Second International Conference on Image, Vision and Computing (ICIVC), IEEE, 783–787, 2017.
- X. Yang, D. Xia, T. Kin, T. Igarashi. Intra: 3d intracranial aneurysm dataset for deep learning. In: Proceedings of the IEEE/CVF Conference on Computer Vision and Pattern Recognition, 2656–2666, 2020.
- Ye, X., Lin, X., Dehmeshki, J., Slabaugh, G., Beddoe, G., 2009. Shape-based computer- aided detection of lung nodules in thoracic ct images. *IEEE Trans. Biomed. Eng.* 56 (7), 1810–1820.
- Yu , H. Liu. Feature selection for high-dimensional data: A fast correlation-based filter solution. In: Proceedings of the Twentieth International Conference on Machine Learning (ICML-03), 856–863, 2003.
- Zafar, Z., Adnan, S.M., Rashid, J., Admad, W., Ikram, J., 2019. Brain tumor detection and classification using geometrical shapes as texture descriptors. *Tech. J. Univ. Eng. Technollogy (UET) Taxila* 24 (1), 83–89.
- Zeng, Y., Liu, X., Xiao, N., Li, Y., Jiang, Y., Feng, J., Guo, S., 2019. Automatic diagnosis based on spatial information fusion feature for intracranial aneurysm. *IEEE Trans. Med. Imaging* 39 (5), 1448–1458.
- Zhai, X., Eslami, M., Hussein, E.S., Filali, M.S., Shalaby, S.T., Amira, A., Bensaali, F., Dakua, S., Abinahed, J., Al-Ansari, A., et al., 2018. Real-time automated image segmentation technique for cerebral aneurysm on reconfigurable system-on-chip. *J. Comput. Sci.* 27, 35–45.
- Y. Zhang ,L. Chen. Ddnet: a novel network for cerebral artery segmentation from mra images. InProceedings of the Twelfth International Congress on Image and Signal Processing, BioMedical Engineering and Informatics (CISP-BMEI), IEEE, 1–5 2019.
- H. Zhao, J. Shi, X. Qi, X. Wang, J. Jia. Pyramid scene parsing network. In: Proceedings of the IEEE Conference on Computer Vision and Pattern Recognition, 2881–2890, 2017.
- Zhou, G., Zhu, Y., Yin, Y., Su, M., Li, M., 2017. Association of wall shear stress with intracranial aneurysm rupture: systematic review and meta- analysis. *Sci. Rep.* 7 (1), 1–8.
- M. Zhou, X. Wang, Z. Wu, J.M. Pozo, A.F. Frangi. Intracranial aneurysm detection from 3d vascular mesh models with ensemble deep learning. In 22nd International Conference, Medical Image Computing and Computer Assisted Intervention–MICCAI 2019, Springer, Shenzhen, China, October 13–17, 2019, Part IV 22, 243–252, 2019.